Supplemental 1

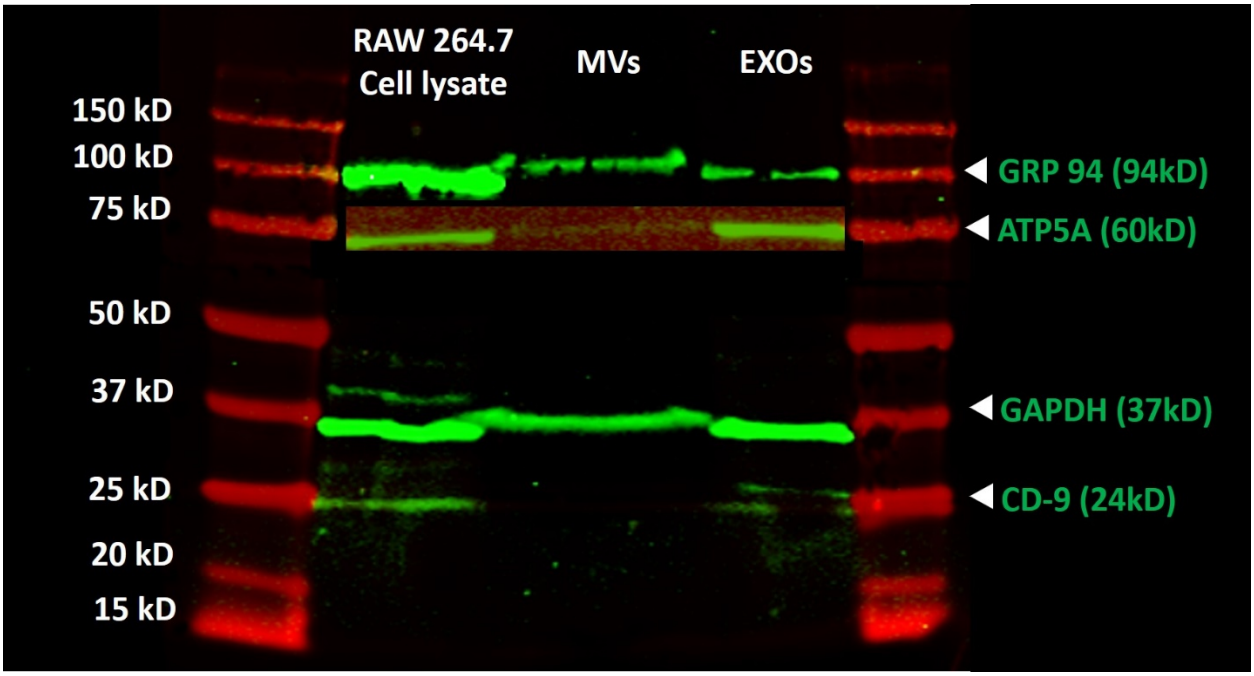

SL. Fig. 1. Detection of characteristic marker proteins in EXOs and MVs-derived from RAW 264.7 cells using western blotting. Each lane was loaded with 25 µg total protein of the indicated sample, electrophoresed, and transferred to a nitrocellulose membrane prior to staining with antibodies to detect GRP94, ATP5A, CD9, and GAPDH proteins. The bands were imaged on the 800 nm channel using an Odyssey imager at intensity setting 5 and processed using ImageStudio 5.2 software.

Cell culture for RAW 264.7 cell line

Abelson murine leukemia virus-transformed macrophages, RAW 264.7, cell line (catalog number. ATCC TIB-71) at passage number (P) 1 was procured from ATCC (Manassas, VA). Cells were maintained in the complete growth medium containing glutamine-supplemented Dulbecco's Modified Eagle's Medium (DMEM (1x) + Glutamax, gibco, Carlsbad, CA) with an added 10% fetal bovine serum. The cells were cultured in a humidified 5% CO_2 incubator at 37 ± 0.5˚C. The old medium was replaced with a fresh complete growth medium every 2 days until about 80% of cell confluency. For subculturing, the cells were washed with PBS (1x) and dissociated from the flask with a sterile cell scraper. The cells were subcultured at the subcultivation ratio from 1:3 to 1:6.

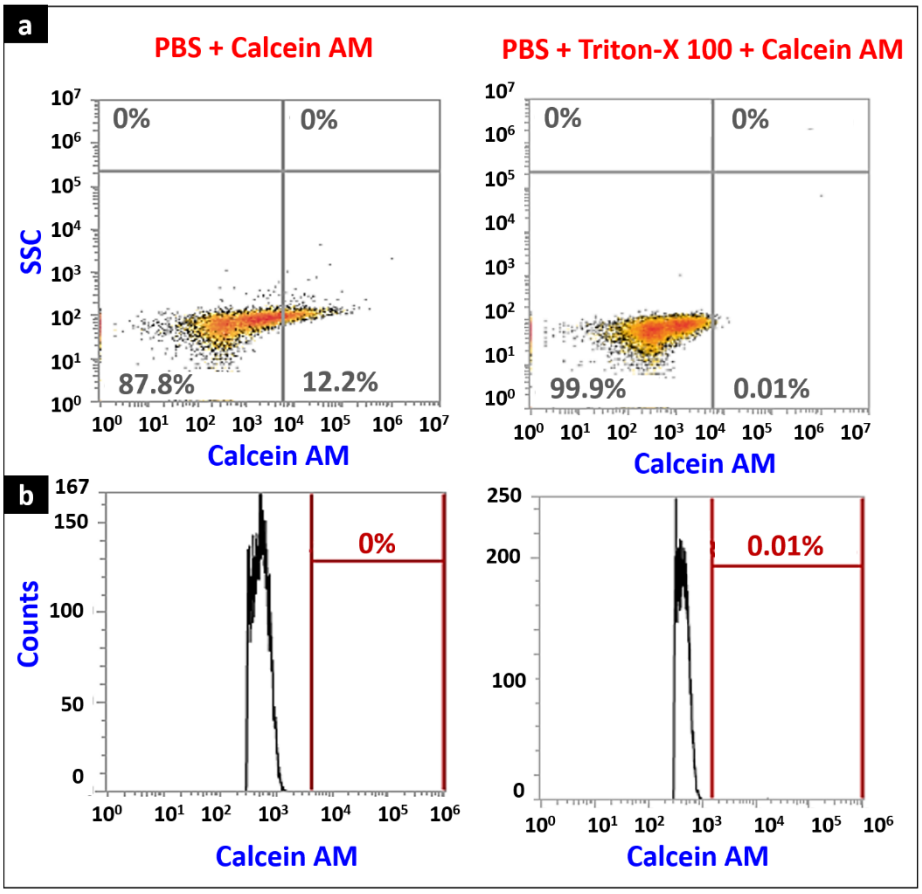

SL. Fig. 2: Flow cytometry plots of processing control samples. The representative density plots (**a**), and histograms (**b**) of PBS/calcein mixture, and PBS/Triton-X 100/calcein mixture.

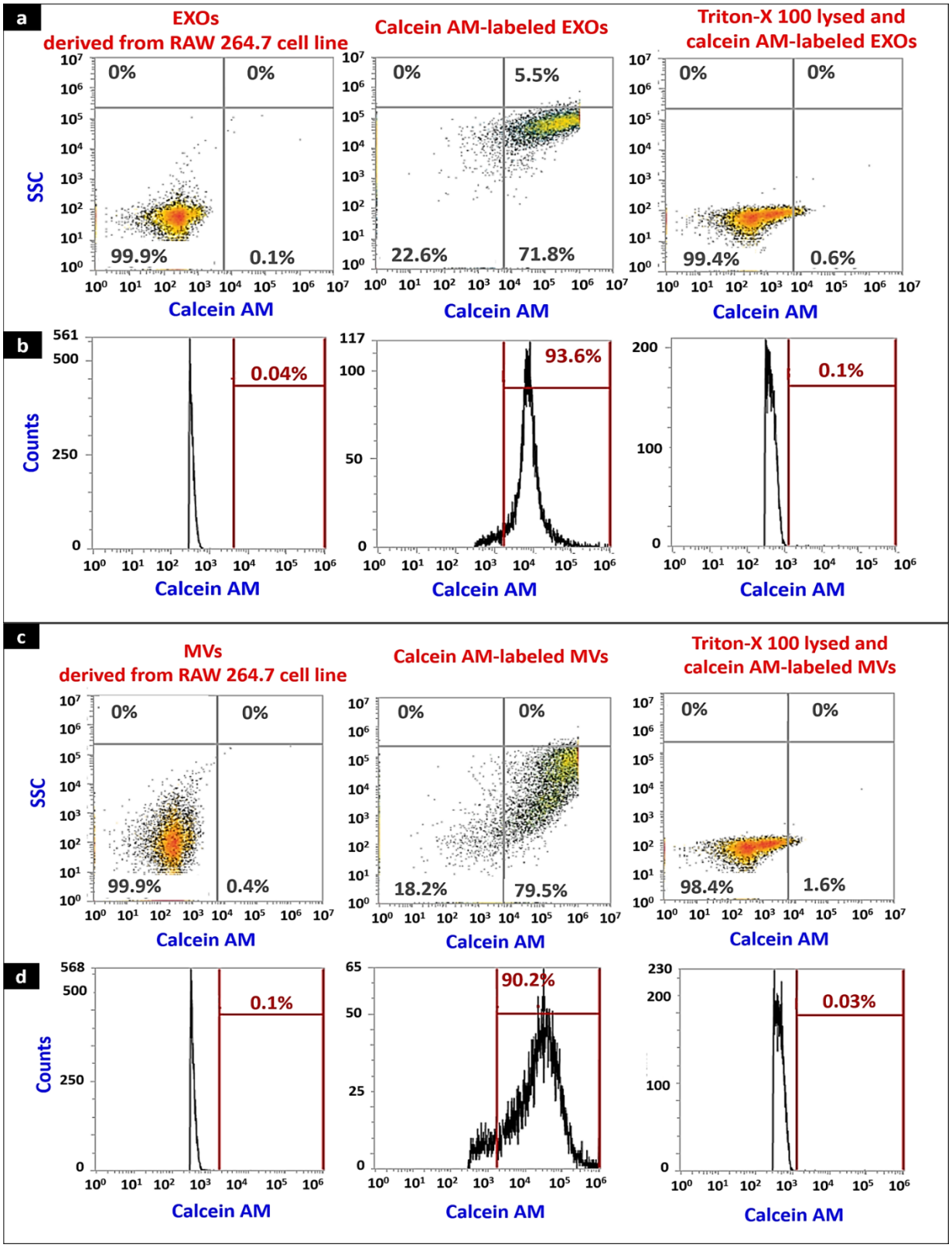

SL. Fig. 3: Integrity of RAW 264.7 cell line-derived EVs after ultracentrifugation and resuspension using flow cytometry. EVs were isolated from RAW 264.7 cell line using

sequential ultracentrifugation and the pellets were resuspended in PBS. EXOs and MVs at 20 μg/mL were labeled with 10 μM calcein AM. In a separate experiment, EVs have lysed with Triton-X 100 solution, and lysed EVs were labeled with calcein AM. An aliquot of each sample was analyzed for calcein-positive EVs using Attune NXT flow cytometer. The representative density plots (**a**), and histograms (**b**) of EXOs, calcein AM-labeled EXOs, and Triton-X 100 lysed calcein-labeled EXOs. The representative density plots (**c**), and histograms (**d**) of MVs, calcein AM-labeled MVs, and Triton-X 100 lysed calcein-labeled MVs. In density plots, X-axis represents the number of calcein-positive events captured in the side scatter 488/10 nm filter (BL1), whereas the Y-axis represents the number of events acquired in the side scatter (SSC). In histograms, X-axis represents the number of calcein-positive events captured in the side scatter 488/10 nm filter (BL1), whereas the Y-axis represents the total count of the events. *The axes scale in these plots were automatically adjusted by the Attune NxT software*. The data shown are representative plots of n=3 samples.

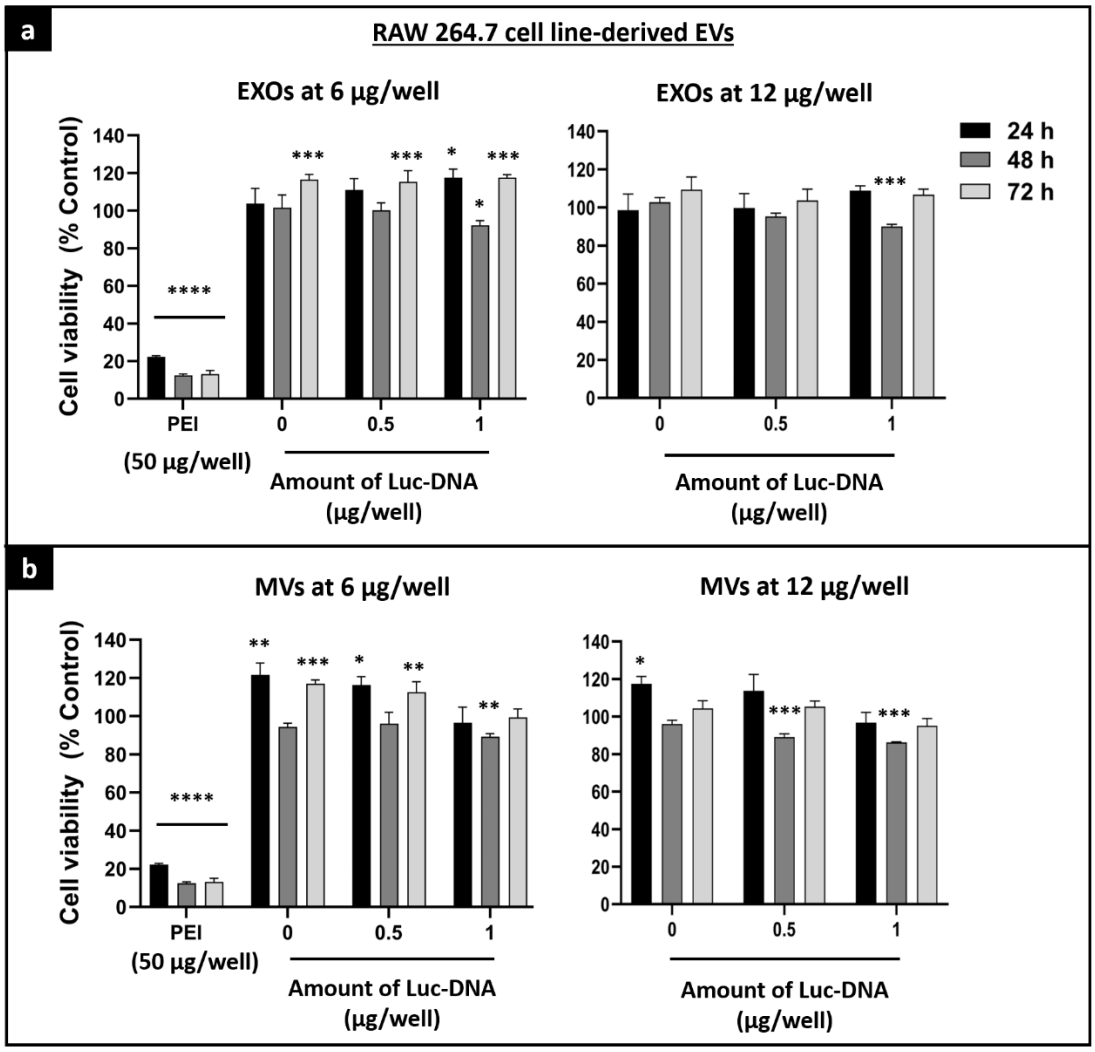

SL. Fig. 4: Cytocompatibility of RAW 264.7 cell line-derived Luc-EVs with hCMEC/D3 cells using ATP assay. hCMEC/D3 cells were seeded in collagen-coated 96-well plates at 16,500 cells/well. At about 80% confluency, hCMEC/D3 cells were incubated with 6 or 12 µg of total EXO protein per well isolated from RAW 264.7 transfected 0, 0.5, or 1 µg Luc-DNA/well plates (**a**), 6 or 12 µg of total MV protein per well isolated from 0, 0.5, and 1 µg Luc-DNA/well plates (**b**), and lipofectamine/Luc-DNA complexes at 10 ng Luc-DNA per well (**c**). EVs were incubated in an incubator for 24, 48, or 72 h, whereas lipofectamine/DNA complexes were incubated for 24 or 48 h. PEI at 50 µg/mL was used as a positive control and untreated cells were also used as a control. Post-incubation, the Cell Titer Glo 2.0 reagent was added to an equal volume of cell culture media. The plate was measured for luminescence at 1s integration time using a Glomax luminometer. The %cell viability of the treated cells was calculated by the (relative luminescence unit (RLU) of treated cells/ RLU of untreated cells) ×100. The significance of treated groups was compared against control using a student's unpaired t-test compared to control or one-way ANOVA and the significance levels are indicated as *p<0.05, **p<0.01, ***p<0.001, and ****p<0.0001.

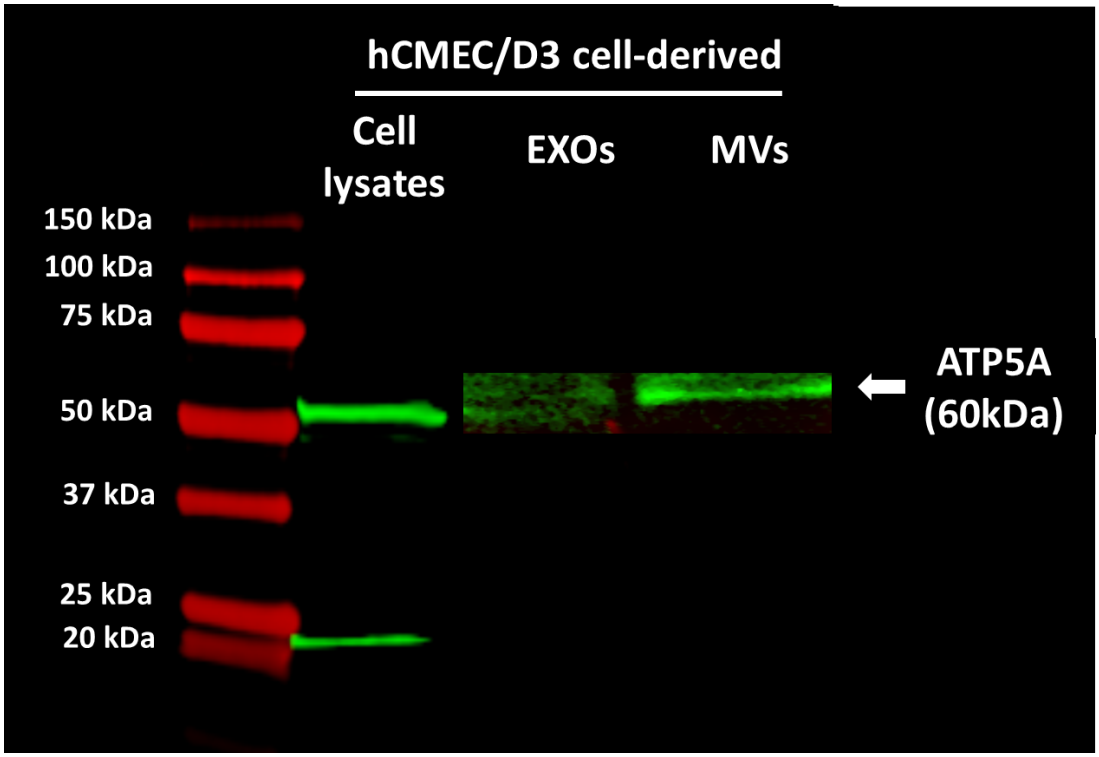

SL. Fig 5: The raw blot of ATP5A detection in EVs using western blotting. Cell lysates at 30 µg/lane and EVs at 50 µg/lane was loaded in 4-10% SDS-PAGE. The gel was run at 120 V for 2 h. The proteins were transferred to a nitrocellulose membrane and blocked with an Odyssey blocking solution for one hour. The membrane was incubated with mouse-derived ATP5A primary antibodies diluted at 1:1000 in the blocking solution and stained with anti-mouse AF790 secondary antibodies diluted at 1:30000 in the blocking solution. The membrane was scanned at 800 nm using an Odyssey infrared imager.

Discussion

Partial specificity of BCA assay for total EV protein content

BCA or MicroBCA assay is not specific to quantity EV protein content, but instead, it measures the total protein content in any given sample. Despite the BCA assay being a non-specific protein assay, it is a rapid, sensitive, and precise method to determine the total EV protein content. We evaluated the correlation between the cell density of the parent cells from which the EVs were isolated and the EV total protein using a Micro BCA assay. For this experiment, we used a fast-growing cell line, spontaneously immortalized microglia (SIM-A9) that we have in the laboratory. This allowed us to rapidly culture the cells and isolate EVs for this experiment. SIM-A9 cells were seeded in 24-well plates where each plate contained 0.1, 0.5, 1, or 5 × 10^5 cells/well/mL and

cultured for 48 h in a humidified incubator (37° C and 5% CO_2). The complete growth medium (DMEM/F12 modified + 10% fetal bovine serum + 5% horse serum) was replaced with one mL of conditioned media (DMEM/F12 modified) in each well and incubated for 48 h. The conditioned media from each plate (24 mL) was pooled into centrifuge tubes and EVs were isolated using a sequential ultracentrifugation method described earlier. The EXOs and MVs pellet was resuspended in 300 µL PBS and the total protein content of a 10 µL aliquot was measured using the micro BCA assay described above. Total protein amount measured from MVs showed a linear increase in total protein with an increase in cell density up to 1×10^5 cells/mL but decreased at 5×10^5 cells/mL (**SL. Fig. 6**). Similarly, total EXO protein content increased with an increase of cell density up to 1×10^5 cells/mL and remained unchanged at 5×10^5 cells/mL (**SL. Fig 6**). The linear increase of total EV protein with the parent cell density suggested that there was a minimal interference of other proteins in EV samples.

We further ran a coomassie gel to demonstrate the correlation between the total protein loading amount in each well and EV proteins. SIM-A9 cell line-derived EXOs and MVs were loaded at 20, 40, and 60 µg/lane in two separate SDS-polyacrylamide gels (4-10%). Pre-mixed protein standards were loaded for the ladder. To evaluate the interference of other proteins, a sample volume equivalent to 60 µg/lane of conditioned media and 40 µg of SIM-A9 cell lysate was analyzed using SDS-PAGE. The gel was run at 120 V for 2 h and stained with 50 mL of coomassie blue staining solution for 1 h. The gel was washed for 1 h with deionized water and scanned at 700 nm and 800 nm using an Odyssey infrared imager.

The gel scanned at 800 nm was depicted in **SL. Fig 7**. With an increase in total protein loading, there was a gradual increase in band density of about 95, 60, and 45 kDa molecular mass proteins (**SL. Fig. 7a and c**). The densitometry analysis showed that there was a linear correlation between the total loaded protein and at least three different MV proteins at 95, 60, and 45 kDa molecular masses (**SL. Fig 7c**). Proteins in the SIM-A9 derived-EXOs at the 20 µg loading amount were below the detection limit (**SL. Fig 7b**). There was a linear increase in 60 kDa protein band density from 40 to 60 µg total loading protein, whereas 80 and 50 kDa proteins showed a small increase in band density (**SL. Fig 7d**). The possible reason could be the constant/non-variable expression of 80 and 50 kDa protein in SIM-A9 cell line-derived EXOs.

To summarise our observations, though the BCA assay is not specific to the EV proteins, it is at least a reliable protein assay to determine the total EV protein content for characterization and transfection experiments. It should be noted that we are aware of this status-quo and our laboratory is currently developing other specific and sensitive assays to quantify EV protein content.

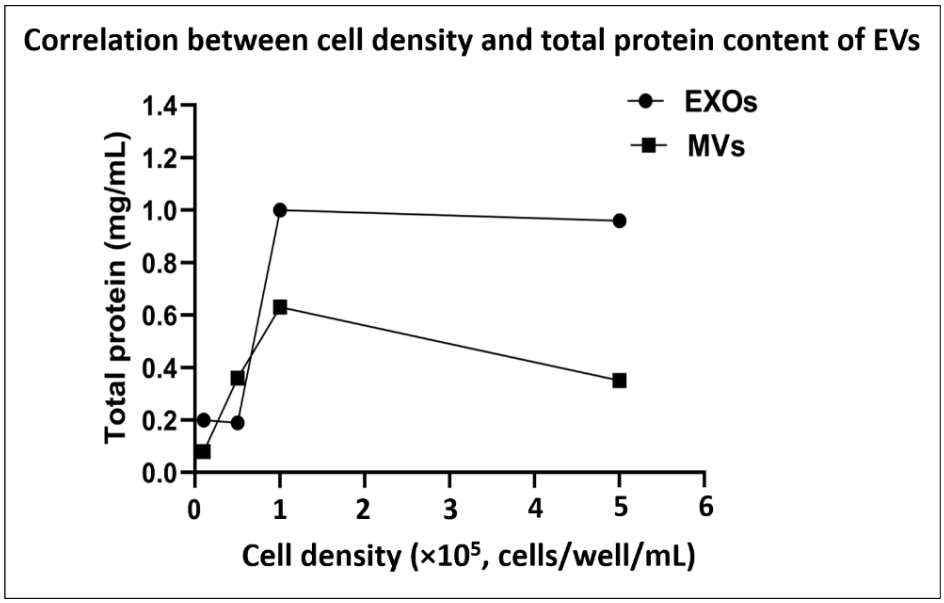

SL. Fig. 6: Correlation between SIM-A9 cell density and the total protein content of their EVs using MicroBCA assay. SIM-A9 cells were seeded at 0.1 – 5 × 10^5 cells/well in 24-well plates and cultured in a complete growth medium for 48 h in a humidified incubator. The complete growth medium was replaced and cells were washed with 1x PBS, following which the cells were incubated with the serum-free medium for 48 h. Post-incubation, the conditioned medium was collected in the corresponding centrifuge tubes, and EVs were isolated using the sequential ultracentrifugation method. EV pellets were resuspended in PBS and total EV protein was measured using MicroBCA assay at 562 nm optical density using a Synergy multi-mode plate reader.

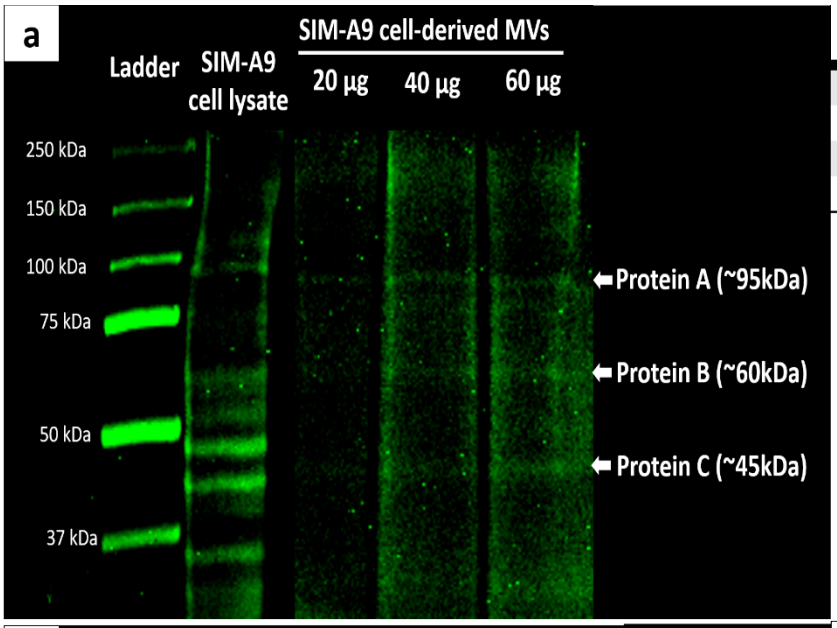

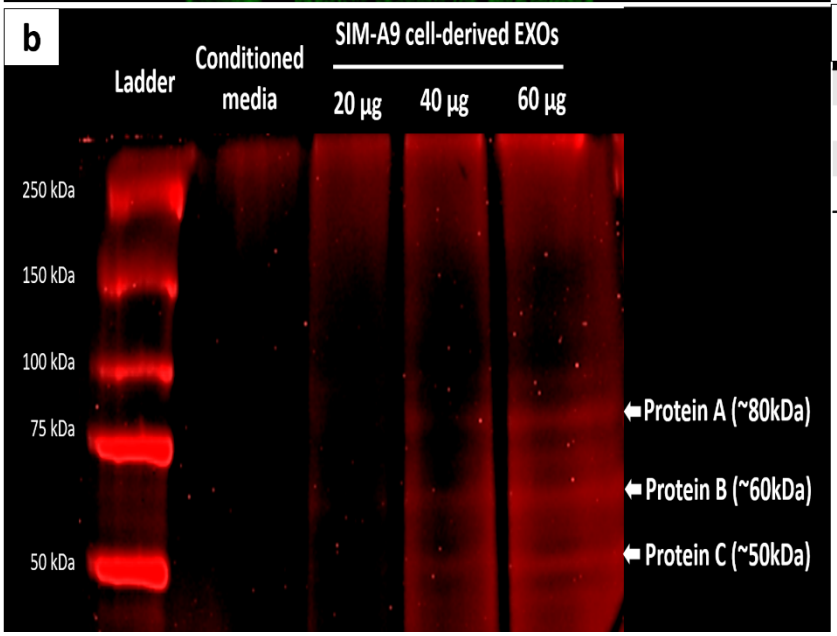

c

	Protein band density (arbitrary units) at total protein amount (µg/lane)		
	20 µg	40 µg	60 µg
Protein A (~95 kDa)	72,800	186,000	242,000
Protein B (~60 kDa)	118,000	265,000	429,000
Protein C (~45 kDa)	118,000	342,000	413,000

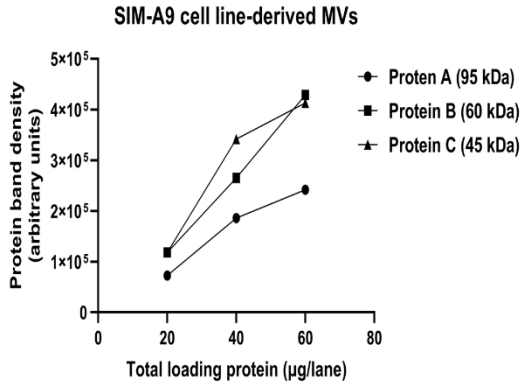

d

	Protein band density (arbitrary units) at total protein amount (µg/lane)		
	20 µg	40 µg	60 µg
Protein A (~80 kDa)	ND	135,000	142,000
Protein B (~60 kDa)	ND	85,800	149,000
Protein C (~50 kDa)	ND	92,400	99,800

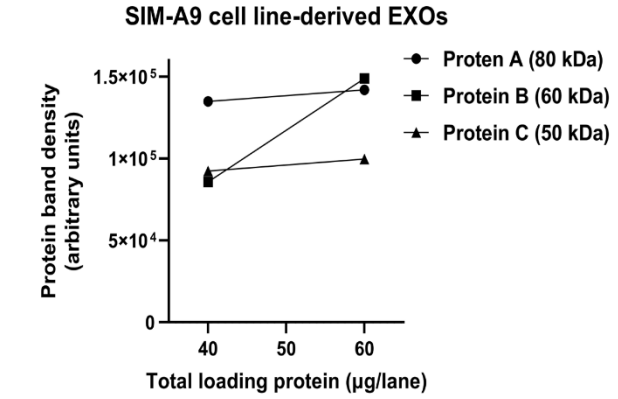

SL. Fig. 7: SDS-PAGE and densitometry analysis of SIM-A9 cell line-derived EVs at increasing amounts of total EV proteins. SIM-A9 cell line-derived MVs (**a**), and EXOs (**b**) were loaded at 20, 40, and 60 µg/lane in 4-10% SDS-PAGE. Ladder, SIM-A9 cell lysates (30 µg/lane), and conditioned medium (volume equivalent to 60 µg/lane total EV proteins) were loaded as molecular markers and processing controls. The gel was run at 120 V for 2 h. The gel was washed with deionized (DI) water and stained with coomassie blue dye for 1 h. The stained gel was washed with DI water and scanned at 700-800 nm using an Odyssey infrared scanner. The identified protein bands (indicated here as proteins A, B, and C) were used for densitometry analysis using ImageStudio 5.2 software. Protein band densities at their arbitrary units were tabulated and a scatter graph depicting total loading protein vs. band densities is shown for selected proteins in the SIM-A9 cell line-derived MVs (**c**), and EXOs (**d**). ND: Not detected.

Perspectives of Engineered EVs for targeted delivery, charge surface modification, and route of administration for ischemic stroke

Approaches to engineer EVs targeted to ischemic stroke

Extracellular vesicles (EVs) can be engineered into targeted drug delivery vehicles that can deliver their cargo to a specific site of action, and hence, can minimize any potential off-target effects. Targeted EVs can be generated via designing and inserting targeting ligands to the surface of EVs using passive or active modification approaches. The passive targeting approaches include a strategic selection and/or manipulation of the EV-producing cells without introducing any alterations to the existing transcriptome (1). EVs produced using a passive approach dependent on the phenotype of parent cells facilitate the homing of EVs towards a specific cell type/ diseased area. For example, Webb *et al.* have demonstrated that the intravenous administration of human neural stem cell (NSC)-derived EVs significantly decreased intracranial hemorrhage, cerebral lesion volume, and brain swelling relative to control groups in ischemic lesions in a pig stroke model (2). The presence of integrin β-1 on NSC EVs facilitates cell-to-cell and cell-to-matrix interactions and migration of EVs, whereas integrin α-2b receptor binds to a variety of ligands resulting in rapid platelet aggregation, leukocyte migration, and megakaryocyte differentiation (2). Collectively, NSC EVs modulated coagulation and vascular functions in the ischemic brain regions resulting in the protection of the blood-brain barrier integrity in the context of stroke therapy (2). Otero-Ortega *et al.* have shown site-specific biodistribution and conducted proteomic analyses of intravenously administered mesenchymal stem cell (MSC)-derived exosomes in an experimental animal model of intracerebral hemorrhage (3). The study demonstrated that systemically administered MSC-exosomes deposited in brain tissue and showed lesion size reduction, axonal sprouting, and an increase in axonal density in the white matter of the striatum. Over 2000 proteins were identified in MSC-exosomes that are implicated in cell function and brain repair function (3). Thus, the selection of parent cells such as NSC, MSC, or macrophages plays a critical role in the passive targeting of the EVs to the ischemic brain regions.

Targeting EVs using a passive approach may not be entirely sufficient since the relative lower abundance or absence of the expression of certain targeting proteins on EV surfaces may render such targeting inefficient. In such cases, an overexpression or recombinant expression of cell transcriptomes using an active targeting strategy may be beneficial. Active targeting can be accomplished by either 1) insertion of a targeting epitope into a wildtype protein expressed on the EVs, 2) conjugation of a fusion protein, or 3) overexpression of wildtype proteins (1). In a landmark study, Alvarez-Erviti *et al*. used wildtype protein Lamp2b and Rabies virus glycoprotein (RVG)-peptide to target acetylcholine receptors in the brain. Authors demonstrated that the systemic administration of EXOs modified with a neuron-specific RVG-peptide delivered exogenously-loaded therapeutic BACE1 siRNA that resulted in ca. 60% knockdown of targeted mRNA and protein in a mouse model of Alzheimer's disease (4). Yang *et al*. showed that the systemic delivery of Lamp2b-RVG peptide inserted and miR-124 loaded exosomes promoted robust cortical neurogenesis after ischemia in a mice focal ischemia model (5). The fusion protein

strategy involves conjugation of the desired domain of the epitope to the host protein instead of whole wild-type proteins (1). Tian *et al.* have chemically conjugated c(RGDyK) peptide to the curcumin-loaded exosome surfaces to target the lesions in ischemic mice brains (6). Intravenous delivery of these exosomes resulted in a strong suppression of cellular apoptosis and inflammatory responses in the lesion region (6). Ohn *et al.* reported that the intravenous administration of EXOs fused with a GE-11 peptide delivered let-7a miRNA targeted to the epidermal growth factor receptor and resulted in significant suppression of tumor growth in a mouse xenograft breast cancer model (7). Lastly, Grapp *et al*. isolated EVs from rat choroidal epithelial cells that overexpressed the folate receptor-α (8). Intracerebroventricular injection of folate-α overexpressing EVs accumulated in the brain parenchyma by crossing the blood-cerebrospinal fluid barrier in the mouse brain (8).

Approaches for engineering positively charged EVs

The outer membrane of EVs is enriched with anionic phospholipids, such as phosphatidylserine, phosphatidylethanolamine, phosphatidylglycerol along with cholesterol, ceramides, and saturated fatty acids (9). The presence of such anionic lipids not only contributes to the negative surface charge of EVs but also seems to play a role in their clearance. Matsumoto *et al.* demonstrated that phosphatidylserine-induced negative surface charge on exosomes enhances the macrophage-mediated blood clearance of B16BL6 murine melanoma cell-derived exosomes (10). Class B scavenger receptor 1 and CD36 proteins present on macrophages bind to negatively-charged surfaces and facilitate uptake of exosomes by circulating macrophages (10).

Engineering EVs with a positive surface charge can allow to bypass the macrophage uptake of EVs in systemic circulation and also enable the electrostatic association of EVs to the negatively-charged cell membranes. Zhupanyn *et al.* have studied the effect of complexing EVs with polyethyleneimine (PEI)/siRNA complexes on the physicochemical parameters of the resulting assemblies and their gene silencing effects *in vitro* and *in vivo* (11). Incubation of EVs with PEI/siRNA complexes for 15 min at room temperature resulted in the formation of EV-modified PEI/siRNA complexes and resulted in a shift of zeta potential from -16.1 mV (EVs) to about 8.5 mV (EV-modified PEI/siRNA complexes). Zhang *et al.* studied the effect of the amount of PEI added to HEK293T cell-derived EVs on the physicochemical characteristics of the formed PEI/DNA/EVs complexes (12). The study showed that the zeta potential of naked DNA and EVs were below -10 mV, and increasing amounts of EVs in the mixture further decreased the zeta potential values (12). Increasing the amounts of PEI resulted in zeta potentials >20 mV of the formed complexes. Increasing the relative amount of EVs at a lower N/P ratio of 2 and 4 of PEI/DNA complexes deceased the overall zeta potential, however, the zeta potential remained unchanged at a higher N/P ratio of 8 to 32 due to the strong cationic charge of the PEI/DNA polyplexes (12).

We determined the changes in the zeta potential of EV membranes upon binding to 25 kDa branched PEI, a synthetic cationic polymer using dynamic light scattering (DLS). EVs (exosomes; EXOs and microvesicles; MVs) were isolated from a spontaneously immortalized microglia (SIM-

A9) and RAW 264.7 cell lines and incubated with 25 kDa PEI to engineer EXO/PEI or MV/PEI complexes. The positively charged amino groups of PEI exert a high charge density under physiological pH (7.4), enabling a strong electrostatic interaction with negatively charged surfaces such as nucleic acids, proteins, and EVs (13). EXOs and MVs at 50 µg/mL were incubated with 0.1, 0.5, and 1 µg/mL PEI dissolved in 10 mM HEPES buffer, pH 7.4 for 20 min at room temperature. The average particle diameter and zeta potential of EVs, free PEI solution, and EV/PEI complexes were measured using a Zetasizer Nano. Each sample was measured thrice, and three independent samples were analyzed. The data are represented as mean ± standard deviation (SD) of triplicate measurements.

SIM-A9 cell line-derived MV and EXO showed a negative zeta potential of about -16.3 and -13.5 mV, respectively (**SL. Table I**). Incubation of EVs with increasing PEI amount showed a considerable shift towards positive zeta potential compared to EVs alone (**SL. Fig. 2a-b**). MV/PEI complexes formed at 0.1 µg/mL PEI showed almost unchanged negative zeta potential (-18.5 mV), however, MV/PEI complexes at 0.5 µg/mL PEI showed a positive zeta potential of 3.5 mV which was further increase to 6.6 mV at 1 µg/mL PEI (**SL. Table I and SL. Fig. 2a**). EXO/PEI complexes at 0.1 µg/mL PEI showed a zeta potential of -0.1 mV. The zeta potential of 0.1, 0.5, and 1 µg/mL PEI solution prepared in 10 mM HEPES buffer, pH 7.4 were ranging from 40 to 60 mV (**SL. Table I and SL. Fig. 2b**). RAW 264.7 cell line-derived MVs and EXOs showed an average zeta potential of -6.8 and -4.5 mV, respectively, which was increased to 7.2 mV and -0.4 mV for MV/PEI and EXO/PEI complexes (**SL. Fig. 2c-d**). Overall, our data is consistent with the previous finding that EV membrane fusion with the cationic synthetic polymers can result in the formation of complexes resulted in altered surface charges for the formed EV/polymer complexes (11, 12).

SL.Table I: Particle size distribution, polydispersity index, and zeta potential of EV, EV/PEI complexes, or PEI solution measured using dynamic light scattering (Malvern Zetasizer Nano). SIM-A9 and RAW 264.7 cell line-derived EVs were suspended at 50 µg/mL in PBS, and PEI was dissolved in 10 mM HEPES buffer pH 7.4 for size, PdI, and zeta potential measurements. PEI at listed concentrations was incubated with EVs for 20 min at room temperature. Data represent the average ± SD of triplicate measurements.

Source of EVs	Sample	Zeta potential (mV)	Particle diameter (nm)	PdI
SIM-A9 cell line	MV	-16.3±3.5	210.4±13.1	0.33±0.07
	MV/PEI complexes (PEI, 0.1 µg/mL)	-18.5±2.9	208.8±24.5	0.33±0.05
	MV/PEI complexes (PEI, 0.5 µg/mL)	3.5±1.1	278.8±44.8	0.44±0.09
	MV/PEI complexes (PEI, 1 µg/mL)	6.6±0.6	521.1±119.9	0.57±0.03
	EXO	-13.5±1.7	156.1±4.4	0.40±0.06
	EXO/PEI complexes (PEI, 0.1 µg/mL)	-0.1±0.3	189.1±43.5	0.31±0.02
	PEI solution, 0.1 µg/mL	43.9±17.3	>2000	0.34±0.26
	PEI solution, 0.5 µg/mL	46.2±2.7	>2000	0.27±0.18

	PEI solution, 1 µg/mL	59.4±16.6	252.7±28.2	0.53±0.21

Source of EVs	Sample	Zeta potential (mV)
RAW 264.7 cell line	MV	-6.8±4.8
	MV/PEI complexes (PEI, 5µg/mL)	7.2±2.2
	EXO	-4.5±2.4
	EXO/PEI complexes (PEI, 5 µg/mL)	-0.4±0.8
	PEI solution, 5 µg/mL	18.1±0.9

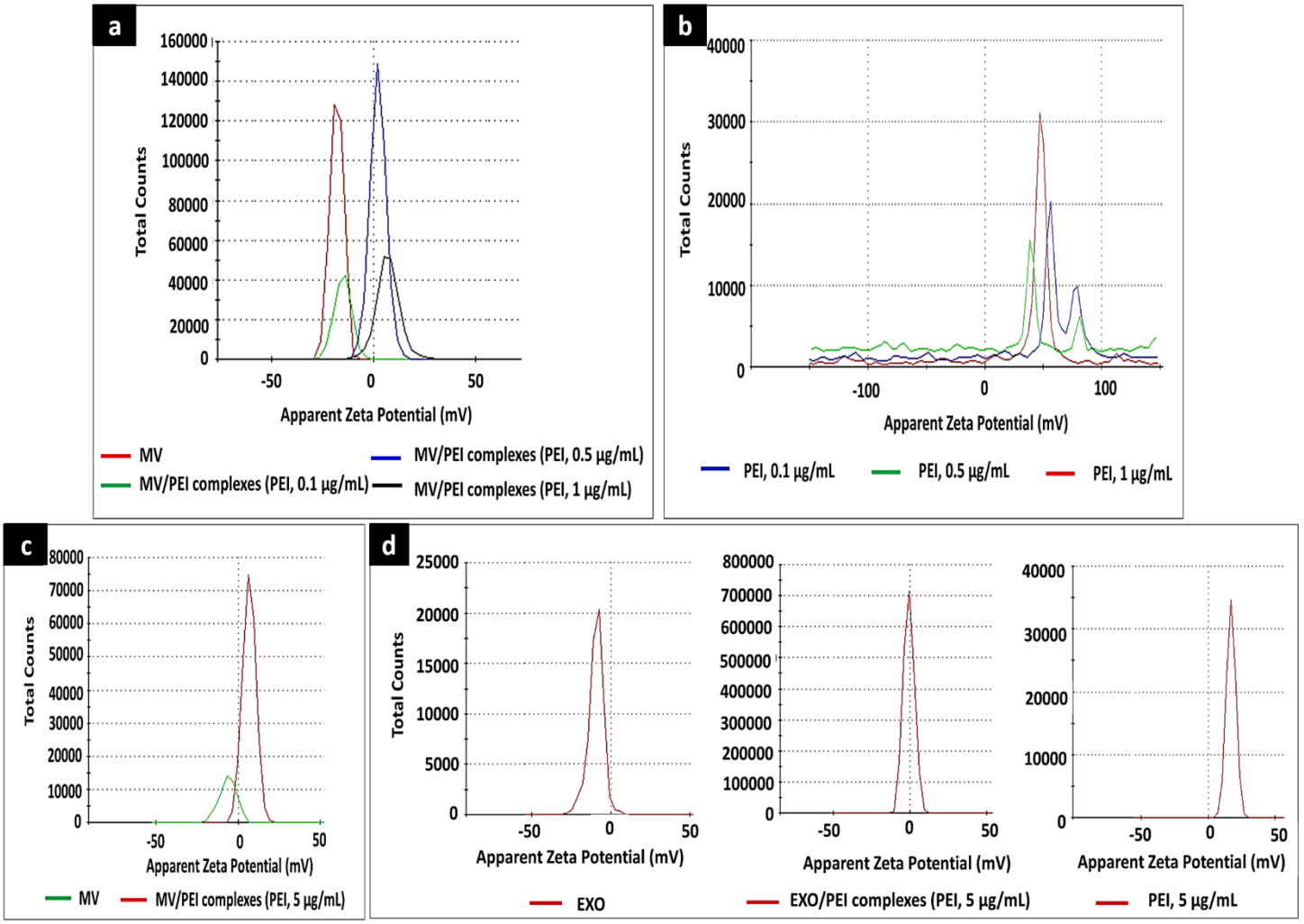

SL. Fig. 8: Apparent zeta potential plots of EV, EV/PEI complexes, and PEI solution. Apparent zeta potential vs. total counts plots of SIM-A9 cell line-derived MVs, and MV/PEI complexes (**a**) PEI solution at 0.1, 0.5, and 1 µg/mL concentration (**b**), RAW 264.7 cell line-derived MVs and MV/PEI

complexes (**c**), RAW 264.7 cell line-derived EXOs, EXO/PEI complexes, and PEI solution at 5 μg/mL concentration (**d**) using Malvern Zetasizer Nano. The plots are representative distributions of the data presented in **SL. Table I** in the supplemental file.

Route of administration for pre-clinical experiments in the ischemic animal model

The route of EV administration for pre-clinical or clinical applications is dependent on the EV uptake mechanism at the site of action. Biomolecular cargoes present in the core and the surface of the EV membranes including nucleic acids, proteins, glycoproteins, and lipidic components contribute an essential role in the interaction between the vesicles and the target cells. A variety of endocytic pathways are involved in EV uptake including caveolin-mediated uptake, macropinocytosis, phagocytosis, and lipid raft-mediated internalization (14). For efficient use of EV as therapeutic biopharmaceuticals for CNS diseases, it is imperative to ensure that EV will reach its target cells in CNS (15). EVs have been reported to reach the blood-brain- barrier (BBB) via the systemic, intranasal, or local route of administration such as intraparenchymal and intracerebroventricular for neurodegenerative disorders. Administration of EVs via intravenous injection is the fastest and most widely-used strategy to deliver drugs to the brain tissues. Systemic administration of EVs has demonstrated successful delivery to different brain conditions suggesting its ability to cross the BBB (16-18). Alvarez-Erviti *et al.* demonstrated that intravenously administered siRNA-loaded EVs derived from dendritic cells were delivered to the brain tissue, resulting in the strong knockdown of BACE1 mRNA and protein knockdown in a mouse model of Alzheimer's disease (4). In other studies, systemically administered multipluripotent mesenchymal stromal cells-derived exosomes promoted functional recovery and neurovascular remodeling in a rat model of traumatic brain injury (19). The internalization of EVs into the brain endothelial cells via micropinocytosis, clathrin-mediated endocytosis, or lipid raft-mediated internalization can be affected by different intracellular mediators and molecular cues, resulting in variabilities in the efficiency and time of EV delivery to cross and/or detect across the BBB (16). Conjugation of targeting ligands such as RVG peptide significantly enhances the EV brain exposure. For example, Yang *et al.* showed that the systemic delivery of Lamp2b-RVG peptide inserted and miR-124 loaded exosomes promoted robust cortical neurogenesis after ischemia in a mice model of focal ischemia (5). The fusion protein strategy involves conjugation of the desired domain of the epitope to the host protein instead of whole wild-type proteins (1). Tian *et al.* chemically conjugated c(RGDyK) peptide to the curcumin-loaded exosome surfaces to target the lesions in ischemic mice brains (6). Intravenous delivery of these exosomes resulted in a strong suppression of cellular apoptosis and inflammatory responses in the lesion region (6). Ohn *et al.* reported that the intravenous administration of EXOs fused with a GE-11 peptide delivered let-7a miRNA targeted to the epidermal growth factor receptor and resulted in significant suppression of tumor growth in a mouse xenograft breast cancer model (7). Intraperitoneal route of EV administration is another common method for EV drug delivery that allows injecting larger EV doses (16).

EV based CNS therapeutic efficacy was also achieved by local delivery options. Didiot *et al.* have shown that unilateral direct brain infusion of siRNA-loaded, glioblastoma-derived exosomes resulted in bilateral Huntington mRNA knockdown in mouse models. Intracerebroventricular injection of folate-α overexpressing EVs accumulated in the brain parenchyma by crossing the blood-cerebrospinal fluid barrier in a mouse brain (8). The intranasal route of administration is also used for EV administration that facilitates EV delivery to the brain, either by entering the circulation by crossing the BBB, or directly through olfactory and trigeminal nerve cells. Bypassing the first-pass metabolism, intranasally administered EV also avoid the intestinal and hepatic accumulation and/or metabolism (16). Haney *et al.* showed a considerable accumulation of macrophage-derived and catalase-loaded exosomes in Parkinson's diseased mouse brains after intranasal administration, resulting in significant neuroprotective effects *in vivo* (20).

In conclusion, intravenous administration of EV showed the potential for therapeutic efficacy in a variety of pre-clinical models and in early phases of clinical trials. In our future animal studies, we will compare biodistribution and endothelia-protective studies of EVs administered via the systemic and intracranial routes in a mouse middle cerebral artery occlusion of ischemic stroke.

References

1. Gudbergsson JM, Jønsson K, Simonsen JB, Johnsen KB. Systematic review of targeted extracellular vesicles for drug delivery – Considerations on methodological and biological heterogeneity. Journal of Controlled Release. 2019;306:108-20.
2. Webb RL, Kaiser EE, Jurgielewicz BJ, Spellicy S, Scoville SL, Thompson TA, et al. Human Neural Stem Cell Extracellular Vesicles Improve Recovery in a Porcine Model of Ischemic Stroke. Stroke. 2018;49(5):1248-56.
3. Otero-Ortega L, Gómez de Frutos MC, Laso-García F, Rodríguez-Frutos B, Medina-Gutiérrez E, López JA, et al. Exosomes promote restoration after an experimental animal model of intracerebral hemorrhage. J Cereb Blood Flow Metab. 2018;38(5):767-79.
4. Alvarez-Erviti L, Seow Y, Yin H, Betts C, Lakhal S, Wood MJA. Delivery of siRNA to the mouse brain by systemic injection of targeted exosomes. Nature Biotechnology. 2011;29(4):341-5.
5. Yang J, Zhang X, Chen X, Wang L, Yang G. Exosome Mediated Delivery of miR-124 Promotes Neurogenesis after Ischemia. Molecular Therapy - Nucleic Acids. 2017;7:278-87.
6. Tian T, Zhang H-X, He C-P, Fan S, Zhu Y-L, Qi C, et al. Surface functionalized exosomes as targeted drug delivery vehicles for cerebral ischemia therapy. Biomaterials. 2018;150:137-49.
7. Ohno S-i, Takanashi M, Sudo K, Ueda S, Ishikawa A, Matsuyama N, et al. Systemically injected exosomes targeted to EGFR deliver antitumor microRNA to breast cancer cells. Mol Ther. 2013;21(1):185-91.
8. Grapp M, Wrede A, Schweizer M, Hüwel S, Galla H-J, Snaidero N, et al. Choroid plexus transcytosis and exosome shuttling deliver folate into brain parenchyma. Nature Communications. 2013;4(1):2123.
9. Konoshenko MY, Lekchnov EA, Vlassov AV, Laktionov PP. Isolation of Extracellular Vesicles: General Methodologies and Latest Trends. BioMed Research International. 2018;2018:8545347.
10. Matsumoto A, Takahashi Y, Nishikawa M, Sano K, Morishita M, Charoenviriyakul C, et al. Role of Phosphatidylserine-Derived Negative Surface Charges in the Recognition and Uptake of Intravenously Injected B16BL6-Derived Exosomes by Macrophages. Journal of Pharmaceutical Sciences. 2017;106(1):168-75.
11. Zhupanyn P, Ewe A, Büch T, Malek A, Rademacher P, Müller C, et al. Extracellular vesicle (ECV)-modified polyethylenimine (PEI) complexes for enhanced siRNA delivery in vitro and in vivo. Journal of Controlled Release. 2020;319:63-76.
12. Zhang Z, Wen K, Zhang C, Laroche F, Wang Z, Zhou Q, et al. Extracellular Nanovesicle Enhanced Gene Transfection Using Polyethyleneimine in HEK293T Cells and Zebrafish Embryos. Frontiers in Bioengineering and Biotechnology. 2020;8(448).
13. Ziebarth JD, Wang Y. Understanding the protonation behavior of linear polyethylenimine in solutions through Monte Carlo simulations. Biomacromolecules. 2010;11(1):29-38.
14. Mulcahy LA, Pink RC, Carter DR. Routes and mechanisms of extracellular vesicle uptake. J Extracell Vesicles. 2014;3.
15. Osorio-Querejeta I, Alberro A, Muñoz-Culla M, Mäger I, Otaegui D. Therapeutic Potential of Extracellular Vesicles for Demyelinating Diseases; Challenges and Opportunities. Frontiers in Molecular Neuroscience. 2018;11(434).

16. Pinheiro A, Silva AM, Teixeira JH, Gonçalves RM, Almeida MI, Barbosa MA, et al. Extracellular vesicles: intelligent delivery strategies for therapeutic applications. Journal of Controlled Release. 2018;289:56-69.
17. Wood MJA, O'Loughlin AJ, Lakhal S. Exosomes and the blood–brain barrier: implications for neurological diseases. Therapeutic Delivery. 2011;2(9):1095-9.
18. Tsilioni I, Panagiotidou S, Theoharides TC. Exosomes in Neurologic and Psychiatric Disorders. Clinical Therapeutics. 2014;36(6):882-8.
19. Yanlu Z, Michael C, Yuling M, Mark K, Hongqi X, Asim M, et al. Effect of exosomes derived from multipluripotent mesenchymal stromal cells on functional recovery and neurovascular plasticity in rats after traumatic brain injury. Journal of Neurosurgery JNS. 2015;122(4):856-67.
20. Haney MJ, Klyachko NL, Zhao Y, Gupta R, Plotnikova EG, He Z, et al. Exosomes as drug delivery vehicles for Parkinson's disease therapy. Journal of Controlled Release. 2015;207:18-30.